

# DIELECTRIC PROPERTIES OF THE QUASI-TWO-DIMENSIONAL ELECTRON LIQUID IN HETEROJUNCTIONS

C. BULUTAY

Department of Electrical and Electronics Engineering,  
Middle East Technical University, Ankara - 06531, TURKEY  
and

M. TOMAK

Department of Physics,  
Middle East Technical University, Ankara - 06531, TURKEY.

## Abstract

A quasi-two-dimensional (Q2D) electron liquid (EL) is formed at the interface of a semiconductor heterojunction. For an accurate characterization of the Q2D EL, many-body effects need to be taken into account beyond the random phase approximation. In this theoretical work, the self-consistent static local-field correction known as STLS is applied for the analysis of the Q2D EL. The penetration of the charge distribution to the barrier-acting material is taken into consideration through a variational approach. The Coulomb form factor that describes the effective 2D interaction is rigorously treated. The longitudinal dielectric function and the plasmon dispersion of the Q2D EL are presented for a wide range of electron and ionized acceptor densities choosing GaAs/AlGaAs as the physical system. Analytical expressions fitted to our results are also supplied to enable a

widespread use of these results.

**PACS:** 71.45.Gm, 73.20.Mf

## 1 INTRODUCTION

The name *electron liquid* or *electron gas* refers to a model system formed by interacting dynamical electrons within a medium containing a uniformly distributed positive charge having no motion. The overall system is electrically neutral. As the positive background is rigid, it does not respond to any kind of excitation, hence, it cannot polarize, however, the electrons can. The three-dimensional (3D) electron liquid (EL) has been studied as a model system for metals [1] and the 3D positive ion liquid was proposed as a model astrophysical system [2]. In the case of two-dimensions, the study of the two-dimensional (2D) EL has been driven mainly by technological advances such as silicon inversion layers [3], modulation doped field effect transistors [4], intercalated graphite layers [5], and fractional quantum Hall effect in 2D electron systems [6]. In addition to its technological importance the 2D EL contains rich physics due to enhanced particle correlations and geometrical parameters that characterize the actual realization of the 2D system.

The EL stayed as a problem of interest in the past few decades and intense research efforts lead to several advances in the field. For the 2D case the first major contribution was due to Stern who calculated the density-density response function of the noninteracting EL [7], which is known in the 3D case as the Lindhard function. The Stern function

(i.e., 2D Lindhard function) immediately made the random phase approximation (RPA) available to 2D EL. RPA was at that time one of the most successful many-body approaches for the EL. In 1976, Jonson [8] showed that for 2D EL, a many-body approach proposed by Singwi and coworkers [9] (referred to as STLS) performed remarkably better than RPA. We have very recently compared the 2D-STLS technique with the quantum Monte Carlo data of Tanatar and Ceperley [10] and proposed analytical forms for the dielectric function of the *ideal* 2D EL based on the STLS technique [11].

The knowledge of the dielectric function and the local-field correction paves the way for a variety of many-body related terms such as self-energy, carrier lifetime, mobility [12]. Connections to density-functional theory can also be established [13]. Furthermore, the dielectric screening plays a substantial role in the characterization of other excitations, such as, polarons [14], [15], [16].

In this work, our aim is to present an accurate and systematic characterization of the dielectric properties of the quasi-2D (Q2D) EL in real heterojunctions where the electron distribution can penetrate to both sides of the interface. The charge distribution is based on a variational approach proposed by Bastard [17]. The effective 2D electron interaction for this system is characterized by the Coulomb form factor. This quantity is treated rigorously. The dielectric function for the GaAs/AlGaAs heterojunction is given for wide ranges of electron and ionized acceptor densities. Throughout this work the term *dielectric function*, refers to the *longitudinal* dielectric function. We also fitted analytical expressions to our data for the efficient use of these results by other researchers.

To simplify the computational labour we stayed in the zero-temperature formulation and the so-called electrical quantum limit, where only the lowest subband along the confinement direction is populated (we refer to a very recent work [18], discussing the effects of higher subbands on the dielectric function).

The paper is planned as follows: Sec. II discusses briefly the variational computation of the Q2D electron distribution. The effective 2D interaction of these Q2D electrons is treated in Sec. III and the modifications to the STLS technique in the Q2D case is contained in Sec. IV. In Secs. V and VI the dielectric function and the plasmon dispersion are considered respectively; all the results are given referring to GaAs/AlGaAs as the physical system, however, the approach is developed for a general heterojunction. In Sec. VII, the fitted analytical expressions for the results are presented. Following the conclusion section, appendices include some details on variational formulation and the Coulomb form factor for a Q2D system.

## **2 VARIATIONAL CHARGE DISTRIBUTION FOR A HETEROJUNCTION**

The electrons from ionized donors in the barrier side of a modulation doped heterojunction are trapped in a wedge-like well formed by a step barrier due to conduction band edge discontinuity on one side, and the potential due to presence of the transferred electrons and ionized acceptors on the other [3]. The one-dimensional quantum confinement

gives the Q2D nature to the system and behaves remarkably different than ideal 2D and 3D systems. In handling the many-body effects in heterojunctions we avoid some critical simplifications that have been used in the past such as infinite barrier height [14], [15], [16] (which is a reasonable approximation only for Si inversion layers) and no ionized acceptors within the channel [19] (which is in fact not the case in practise). For an accurate account of the electronic distribution in heterojunctions, we use Bastard's variational approach that was tested previously in determining the subband energies [17].

The electronic wave function  $\varsigma_i(z)$ , within the effective mass approximation satisfies the one-dimensional Schrödinger equation along the confinement direction (chosen to be the  $z$ -direction)

$$\left[ \frac{-\hbar^2}{2} \frac{d}{dz} \frac{1}{m(z)} \frac{d}{dz} + U_{e-e}(z) + U_A(z) + U_{barrier}(z) \right] \varsigma_i(z) = E_i \varsigma_i(z). \quad (1)$$

$U_{e-e}(z)$  is the potential (energy) formed by the presence of the electrons,  $U_A(z)$  is the potential due to ionized acceptors and  $U_{barrier}(z)$  is a step-barrier potential:  $U_{barrier}(z) = U_b \Theta(-z)$ , resulting from the conduction band edge mismatch of the neighbouring materials.  $m(z)$  is the effective mass of the conduction band electrons being equal to  $m_B$  in the barrier-acting material and  $m_A$  in the well-acting material. Bastard proposed the following variational form for the lowest subband  $\varsigma_1(z)$  allowing penetration to the barrier region, ( $z < 0$ ) [17]

$$\varsigma_1(z) = \begin{cases} M e^{\kappa_b z/2}, & \text{for } z \leq 0 \\ N(z + z_0) e^{-bz/2}, & \text{for } z \geq 0 \end{cases}. \quad (2)$$

Invoking the continuity of  $\varsigma_1(z)$  and  $m^{-1}(z)\frac{d}{dz}\varsigma_1(z)$  at  $z = 0$  and the normalization of  $\varsigma_1(z)$ ,  $\int_{-\infty}^{+\infty} dz |\varsigma_1(z)|^2 = 1$ , yields the following three equations,

$$M = Nz_0, \quad (3)$$

$$z_0 = \frac{2}{b + \kappa_b \frac{m_A}{m_B}}, \quad (4)$$

$$N = \sqrt{\frac{b^3}{2 \left[ 1 + bz_0 + \frac{b^2 z_0^2}{2} \left( 1 + \frac{b}{\kappa_b} \right) \right]}}. \quad (5)$$

Bastard also set  $\kappa_b = 2\sqrt{2m_B U_b/\hbar^2}$  and used  $b$  as the only variational parameter. We have observed that such a choice of  $\kappa_b$  is highly satisfactory in the electrical quantum limit. Note that  $M, N$  and  $z_0$  also depend on  $b$  through Eqs.(3)-(5).  $b$  is determined by minimizing the *total* system energy (see Appendix A for the expressions). A closed form representation of  $b$  is not possible, unlike the Si-inversion layer [3], however, the minimization can easily be achieved numerically. We work in the regime where only the lowest subband is populated, this puts an upper limit to the 2D electron density above which the Fermi level crosses the first-excited subband energy. For GaAs/AlGaAs heterojunction our analysis is valid for the 2D electronic densities,  $N_{2D} \leq 7 \times 10^{11} \text{ cm}^{-2}$ . Bastard's work [17] can be consulted for further details.

### 3 COULOMB FORM FACTOR FOR A PENETRABLE HETEROJUNCTION

In the 2D EL the interaction potential in reciprocal space is taken to be  $2\pi e/q$ , where  $q$  is the wave number. This potential is obtained by taking the 2D Fourier transform of the 3D Coulomb interaction which is  $1/R$ ,  $R$  denoting distance in real space [20]. In fact a strictly 2D solution of Poisson's equation is proportional to  $-\ln(R)$  [21] rather than  $1/R$  and its 2D Fourier transform is proportional to  $1/q^2$  as in 3D EL. However, the  $-\ln(R)$  interaction is seldom used [22] due to indication by real physical 2D systems that  $1/R$  type of interaction is relevant [23],[24]. For the case of a Q2D system the charge distribution along the third dimension modifies the effective 2D interaction from  $2\pi e/q$  to  $F(q) 2\pi e/q$ .  $F(q)$  is the Coulomb form factor describing the effect of the finite spread of the charge distribution along the confinement direction over a region where the background dielectric constant is discontinuous due to different materials on both sides.

Following the approach in the previous section we use the variational charge distribution that can leak into the barrier region and calculate the function  $F(q)$  accordingly. The details on  $F(q)$  are given in the Appendix B, here we state the final result,

$$F(q) = \frac{1}{2} \left(1 + \frac{\epsilon_B}{\epsilon_A}\right) I_1 + \frac{1}{2} \left(1 - \frac{\epsilon_B}{\epsilon_A}\right) I_2 + \frac{1}{2} \left(1 + \frac{\epsilon_A}{\epsilon_B}\right) I_3 + \frac{1}{2} \left(1 - \frac{\epsilon_A}{\epsilon_B}\right) I_4 + 2I_5, \quad (6)$$

where,

$$I_1 = 2N^4 \left\{ \frac{1}{2b} \left[ \frac{z_0^4}{(b+q)} + \frac{2z_0^3}{(b+q)^2} + \frac{2z_0^2}{(b+q)^3} \right] + \frac{1}{(2b)^2} \left[ \frac{4z_0^3}{(b+q)} + \frac{6z_0^2}{(b+q)^2} + \frac{4z_0}{(b+q)^3} \right] \right\}$$

$$+ \frac{1}{(2b)^3} \left[ \frac{12z_0^2}{(b+q)} + \frac{12z_0}{(b+q)^2} + \frac{4}{(b+q)^3} \right] + \frac{1}{(2b)^4} \left[ \frac{24z_0}{(b+q)} + \frac{12}{(b+q)^2} \right] + \frac{1}{(2b)^5} \frac{24}{(b+q)} \left. \right\}, \quad (7)$$

$$I_2 = N^4 \left[ \frac{z_0^2}{(b+q)} + \frac{2z_0}{(b+q)^2} + \frac{2}{(b+q)^3} \right]^2, \quad (8)$$

$$I_3 = \frac{M^4}{\kappa_b(\kappa_b + q)}, \quad (9)$$

$$I_4 = \frac{M^4}{(\kappa_b + q)^2}, \quad (10)$$

$$I_5 = \frac{M^2 N^2}{(\kappa_b + q)} \left[ \frac{z_0^2}{(b+q)} + \frac{2z_0}{(b+q)^2} + \frac{2}{(b+q)^3} \right]. \quad (11)$$

In Eq. (6)  $\epsilon_A$  and  $\epsilon_B$  are the background dielectric constants of the well-acting and the barrier-acting materials respectively. The bare electron-electron interaction potential energy for this Q2D system becomes

$$U^{Q2D}(q) = \frac{2\pi e^2}{\bar{\epsilon} q} F(q) \quad (12)$$

where  $\bar{\epsilon} = (\epsilon_A + \epsilon_B)/2$  and  $q$  is the 2D wave number associated with the spatial variation along the 2D sheet.

The terms containing  $I_2$  and  $I_4$  in Eq. (6) represent the image interaction resulting from the different permittivities on both sides. Their effects decrease when the permittivity contrast diminishes; an example is the GaAs/AlGaAs system considered in Fig. 1 for two different electron densities (see the following section for the material parameters used). The Coulomb form factor becomes more important in high electron densities (see Fig. 1) where the in-plane particle separation is comparable to the extension of the charge distribution along the confinement direction. The expression for  $F(q)$  in Eq. (6) will especially be useful for heterojunctions with a high permittivity difference and a low barrier height.

## 4 Q2D STLS

The STLS technique in 2D has been discussed in the literature, and we refer, for instance, to Jonson's pioneering paper [8]. In going from 2D to Q2D the only modification (within the electrical quantum limit) is the replacement of the 2D Coulomb interaction energy by the effective 2D interaction due to finite extension of the charge distribution along the confinement direction. The exchange and correlation hole associated with each electron in the system is described by the local-field correction,  $G(q)$ . This function in the case of Q2D STLS reads

$$G^{Q2D}(q) = \iint \frac{d^2 p_n}{2\pi} \frac{F(p)}{F(q)} \frac{\vec{q}_n \cdot \vec{p}_n}{q_n p_n} [1 - S(|\vec{p} - \vec{q}|)], \quad (13)$$

where the subscript  $n$  is used in this equation and in the rest of the text to denote wave numbers normalized to the Fermi wave number  $k_F$  (i.e.,  $q_n \equiv q/k_F$  etc.). In Eq. (13)  $F$  is the Coulomb form factor and  $S$  is the static structure factor. The latter contains contributions from plasmons and electron-hole pairs and is related to the dielectric function through the fluctuation-dissipation theorem. The dielectric function, in turn, depends on the local-field correction (see Sec. V). The computational task involves the self-consistent solution of these three coupled nonlinear integral equations. A change of variables leads to a substantial improvement in the execution speed of the STLS algorithm. Using  $\vec{t}_n = \vec{p}_n - \vec{q}_n$  in Eq. (13) leads to

$$G^{Q2D}(q) = \frac{1}{\pi F(q)} \int_0^\infty dt_n t_n [1 - S(t)] \int_0^\pi d\phi F\left(q\sqrt{1 + a^2 + 2a \cos \phi}\right) \frac{a \cos \phi + 1}{\sqrt{1 + a^2 + 2a \cos \phi}}, \quad (14)$$

where  $a = t_n/q_n$ .

In Fig. 2 we present the self-consistent STLS  $G^{Q2D}(q)$  results for a wide range of electronic densities given in terms of  $r_s$ .  $r_s$  is the effective interparticle spacing defined as  $r_s = 1/a_B^* \sqrt{\pi N_{2D}}$  where  $N_{2D}$  is the 2D electronic density and  $a_B^*$  is the effective Bohr radius given by  $a_B^* = \frac{\bar{\epsilon}}{m^*} \frac{\hbar^2}{m_0 e^2}$ ,  $\bar{\epsilon}$  is the background average static dielectric constant and  $m^* m_0$  is the effective mass of the electrons considered, with  $m_0$  being the free electron mass. We consider GaAs/AlGaAs heterojunction as the physical system with the parameters  $m_A = 0.07m_0$ ,  $m_B = 0.088m_0$ ,  $\epsilon_A = 13$ ,  $\epsilon_B = 12.1$  and  $U_b = 0.3$  eV (corresponding to an Al mole fraction of 0.3) which were used by Stern and Das Sarma [25]. For  $a_B^*$  we used  $\bar{\epsilon} = 12.55$  and  $m^* = 0.07$ , giving  $a_B^* = 9.49$  nm. The conduction band offset,  $U_b$  was measured by some groups to be around 0.225 eV (in contrast to 0.3 eV) [26]. We have observed that our results are not sensitive to the deviation of  $U_b$  in this range. In Fig. 2 the interval  $r_s = 0.8 - 20$  is shown with an ionized acceptor density of  $N_{depl} = 0.46 \times 10^{11} \text{ cm}^{-2}$ . For  $r_s < 0.8$  the higher subbands start to be populated which was not taken into our analysis.

For the 2D EL, STLS  $G(q)$  becomes proportional to  $q$  as  $q \rightarrow 0$  [11] whereas in 3D case it is proportional to  $q^2$  [1]. In the Q2D case we observe that (see Fig. 2) for low  $r_s$  values small- $q$  behavior is close to quadratic and as  $r_s$  increases this behavior goes towards a linear one indicating an approach to a 2D character.

Gold and Calmels also reported their results on  $G^{Q2D}(q)$  for GaAs/AlGaAs heterostructure [19]. Their treatment is based on STLS but with essential discrepancies compared to ours. They imposed the local-field correction for 2D and Q2D to be of the

form

$$G_{GC}^{Q2D}(x) = r_s^{2/3} \frac{1.402 x}{[2.644 C_{12}^2(r_s) + x^2 C_{22}^2(r_s)]^{1/2}} \quad (15)$$

where  $x = \frac{q}{k_F} \frac{1}{\sqrt{2} r_s^{1/3}}$  and the coefficients  $C_{12}$  and  $C_{22}$  were tabulated [19]. They assumed no penetration to barrier region in the Coulomb form factor and also neglected the presence of ionized acceptors in the well-acting region. Especially, the form used in Eq. (15) enabled them to reduce the computational effort appreciably, however, their results are in strong disagreement with ours for  $r_s \geq 1$  and  $q \simeq 2k_F$  both in 2D [11] and Q2D as can be seen in Fig. 3. The form in Eq. (15) cannot accommodate the full STLS  $G(q)$  leading to a poor dielectric function and screening properties. The ionized acceptors in the well region play a primary role and need to be included in the treatment.

## 5 DIELECTRIC FUNCTION

The function of practical importance is the wave number- and frequency-dependent (longitudinal) dielectric function,  $\epsilon(q, \omega)$  that not only determines the response to a weak external perturbation but also possesses information on the many-body dynamics of the system. With the knowledge of the local-field correction,  $\epsilon(q, \omega)$  is given as

$$\epsilon_{STLS}^{Q2D}(q, \omega) = \frac{1 - U^{Q2D}(q) \pi^0(q, \omega) [1 - G^{Q2D}(q)]}{1 + U^{Q2D}(q) \pi^0(q, \omega) G^{Q2D}(q)}, \quad (16)$$

where  $\pi^0(q, \omega)$  is the 2D zeroth-order polarization insertion, the Stern function [7], [11].

Apart from  $\pi^0$ , 2D and Q2D quantities behave differently. This is illustrated in Fig. 4 showing inverse static dielectric function,  $\epsilon^{-1}(q, 0)$  within RPA and STLS for both 2D

and Q2D cases. To assess the effect of penetration of the charge distribution into the barrier region, we compare  $U_b = 0.1 \text{ eV}$  case with  $U_b \rightarrow \infty$  in Fig. 5 at  $r_s = 0.8$ . It is observed that for GaAs/AlGaAs-like heterojunctions, this penetration has a minor effect on the static dielectric function. In Fig. 6 the inverse static dielectric function of GaAs/AlGaAs heterojunction is plotted in the density range  $r_s = 0.8 - 20$  and for  $N_{depl} = 0.46 \times 10^{11} \text{ cm}^{-2}$ . Notably, the GaAs/AlGaAs heterostructure shows an overscreening effect (i.e.,  $\epsilon < 0$ ) for  $r_s \geq 3$ . The onset of overscreening shifts to higher electron densities for the strictly 2D case [11], due to enhanced particle correlations in lower dimensions. As an interesting consequence, the negative dielectric function suggests a negative compressibility of the Q2D EL [12] and in fact, recently this has been experimentally observed on a GaAs quantum well structure [27].

We would like to include some necessary remarks about this dielectric function. The expression in Eq. (16) only gives the Q2D EL dielectric function. The total screened electron-electron interaction is

$$U_{scr}^{Q2D}(q, \omega) = F(q) \frac{2\pi e^2}{\bar{\epsilon} q} \frac{1}{\epsilon_{STLS}^{Q2D}(q, \omega)}. \quad (17)$$

The dielectric responses of the polar lattice and the valence electrons are contained in the average background dielectric constant  $\bar{\epsilon}$ . Here we have used the *static* dielectric constant (see, for instance, our definition of  $a_B^*$  in Sec. IV), hence, it is assumed that the polar lattice can follow the external excitations. Obviously this limits the validity range of this work to  $\omega \ll \omega_{TO}$ , with  $\omega_{TO}$  being the transverse optical phonon frequency. This limitation is relaxed if the background lattice does not have a polar character. Hence,

for the particular system that we are considering, the dielectric function is expected to be valid up to about 1 THz. In principle, however, the static nature of the local field correction of the STLS technique can further limit this upper frequency.

Finally, the dielectric function given by Eq. (16) takes into account the polarization of the electrons in the lowest subband. Even though the presently available experiments on GaAs/AlGaAs systems mainly fall into this regime [28], [29], the technological trend aims to populate the higher subbands to increase the amount of current carried in modulation doped field effect transistors by using different materials such as InGaAs/InAlAs [4]. When the higher subbands are occupied the dielectric function should necessarily be a tensor of the form  $\epsilon_{ij}(q, \omega)$ , where  $i = j$  terms account for the intrasubband polarizations and  $i \neq j$  terms represent intersubband couplings. To assess the performance of the presented approach regarding the electrical quantum limit, we extended the variational wave function technique to include lowest two subbands and determined the subband populations by invoking self-consistency between Poisson and Schrödinger equations. In Fig. 7 we show the charge distributions along the confinement direction for a density of  $1 \times 10^{12} \text{ cm}^{-2}$ . The solid curve represents the correct charge distribution containing contributions from the lowest and first-excited subbands. The dashed curve, on the other hand, sticks to the electrical quantum limit which actually breaks down beyond  $N_{2D} = 7 \times 10^{11} \text{ cm}^{-2}$ . It is important to observe that the difference between the two curves is quite marginal. This is simply because the percentage of the first-excited subband electrons is 4.7% at this density.

## 6 PLASMON DISPERSION

The elementary excitations in electron liquids are electron-hole pair creations and collective excitations known as plasmons [30]. The latter can be characterized with the knowledge of the wave number and frequency-dependent dielectric function,  $\epsilon(q, \omega)$ . Particularly, the plasmon dispersion relation,  $\omega_p(q)$  is available through the zeros of the dielectric function;

$$\epsilon(q, \omega_p(q)) = 0. \quad (18)$$

Inserting the expression for  $\epsilon(q, \omega)$  from Eq. (16) leads to the following closed form expression for the plasmon dispersion

$$\nu_p(q) = \frac{q_n(z+1)}{2} \sqrt{q_n^2 + \frac{4}{z^2 + 2z}}, \quad (19)$$

where

$$z = \frac{q_n}{\sqrt{2}r_s F(q) [1 - G^{Q2D}(q)]}, \quad (20)$$

and

$$\nu_p(q) = \frac{\hbar\omega_p(q)}{2E_F} = \frac{m\omega_p(q)}{\hbar k_F^2}. \quad (21)$$

which is valid in the range  $[0, q_{n,max}]$  where  $q_{n,max}$  satisfies  $\nu_p(q_{n,max}) = q_{n,max} + q_{n,max}^2/2$  and outside this region plasmons dissociate to electron-hole pairs so that collective excitations are no longer long-lived. The Eq. (19) reduces to the ideal 2D result [31] when  $F(q) \rightarrow 1$ . Fig. 8 shows the plasmon dispersion for GaAs/AlGaAs heterostructure with  $N_{depl} = 0.46 \times 10^{11} \text{cm}^{-2}$  and for several  $r_s$  values. Even though the plasmon dispersion

can be experimentally probed, such as, through far infrared spectroscopy [28], the available experimental results pertain to high electronic densities and small wave numbers ( $q < k_F$ ). Therefore the effects of the local-field correction have not yet been verified.

## 7 ANALYTICAL EXPRESSIONS

In this section we present our fitted expressions to  $G^{Q2D}(q)$  and  $F(q)$  applicable to GaAs/AlGaAs heterojunction in the density range  $r_s = 0.8 - 20$ . As a fit to  $G^{Q2D}(q)$  (shown in Fig. 2 by solid lines), we tried a simple form containing three fitting parameters,

$$G_{fit}^{Q2D}(q) = A \left( 1 - e^{-\frac{B}{A} q^C} \right), \quad (22)$$

where  $A, B$  and  $C$  are the fitting parameters. The optimized values are tabulated in Table I for  $N_{depl} = 0.46 \times 10^{11} \text{ cm}^{-2}$ . The third parameter,  $C$  is introduced based on our observations on the long-wavelength behavior of  $G^{Q2D}(q)$  in Sec. IV. In ideal 2D,  $C$  was equal to one and in 3D case  $C$  was equal to two. Optimized  $C$  values in Table I show this interpolation between  $r_s = 0.8$  to 5, but then this trend is lost to enable a good fit for the whole  $q$  values. The fitted expressions are plotted in Fig. 2 by the dotted lines. To assess the quality of the fitting we use the following error estimate between a target vector,  $T(i)$  and the fitted vector  $T_{fit}(i)$ :

$$error(\%) = \frac{1}{N} \sum_{i=1}^N \left| \frac{T(i) - T_{fit}(i)}{T(i)} \right| 100. \quad (23)$$

Accordingly the deviation of the fitting in Fig. 2 is less than 2.5 %.

The Coulomb form factor,  $F(q)$  also requires a laborious work for GaAs/AlGaAs system. This function can be fitted by a simple expression

$$F_{fit}(q) = \frac{1}{1 + Dq_n}, \quad (24)$$

containing a single fitting parameter  $D$  which is tabulated in Table I for the same  $N_{depl}$  value.

The knowledge of  $G_{fit}^{Q2D}(q)$  and  $F_{fit}(q)$  is sufficient for representing the dielectric function (see Eq. (16)). The performance of fitting for  $\epsilon^{-1}(q, 0)$  is available from Fig. 6 (shown by dotted lines) where the error, using the estimate in Eq. (23) is less than 1%. Similarly in Fig. 8 the plasmon dispersions with the use of the fitted forms are shown in dashed lines, the fitting error being much less than 0.1%.

We have observed that taking the barrier height  $U_b = 0.225$  eV does not significantly affect the parameters  $A, B, C$ , and  $D$ . However,  $N_{depl}$  takes an important part in both  $G(q)$  and  $F(q)$ , so we repeated the self-consistent Q2D STLS technique for  $N_{depl} = 0.146, 1.47, 4.69 \times 10^{11} \text{ cm}^{-2}$  and performed again fittings. Rather than specifying these results in tabular form we present below fitted *functions* of  $r_s$  for  $A, B, C$ , and  $D$ .

$$A_{fit} = 1.02 \left[ 1 - a_1 r_s^{a_2} e^{-a_3 r_s} \right], \quad (25)$$

$$B_{fit} = b_1 \ln(b_2 r_s) + b_3, \quad (26)$$

$$C_{fit} = 0.42 r_s^{-c_1} + 1.03 r_s^{0.12}, \quad (27)$$

$$D_{fit} = \frac{d_1}{d_2 + r_s^{1.15}}, \quad (28)$$

the constant parameters contained in these expressions are tabulated in Table II for the considered range of  $N_{depl}$  values. With the expressions in Eqs. (25)-(28), inverse static dielectric function can be generated to an accuracy of about 1 % except  $r_s = 2$  case having an error about 9 %. Similarly with these equations plasmon dispersion can be recovered to an error much less than 0.1 %.

## 8 CONCLUSION

The dielectric properties of the Q2D EL in a heterostructure are studied and the behaviour is seen to be remarkably different than the strictly 2D EL [11]. The analysis is rigorous with the only simplifications being the electrical quantum limit and the zero-temperature formalism. These simplifications can also be relaxed at the expense of computational complexity. The leakage of the charge distribution to the barrier region is included in the analysis through a variational approach. The full form of the Coulomb form factor applicable to a general heterostructure is presented. For the GaAs/AlGaAs system, the image terms have been observed to have a marginal role. A sizeable contribution will be encountered in the case of heterostructures built up of materials having a high dielectric constant contrast and a low conduction band offset. The dielectric function and the plasmon dispersion of the Q2D EL are characterized using the STLS many-body approach that leads to substantial improvement over the conventional RPA. Unfortunately, in contrast to the ideal 2D case [10], [32], quantum Monte Carlo simulations are not available, to compare our results, for the Q2D EL; the present experimental

data cannot cover the regime where the RPA breaks down (i.e.,  $r_s > 1$  and  $q \simeq k_F$ ). Our analysis extends to a wide range of electron and ionized acceptor densities. To the best of our knowledge this work forms the most elaborate study of the screening properties of the Q2D EL. Our results are supplemented with analytical expressions fitted to our data. We have presented the expressions for the local-field correction, Coulomb form factor, the dielectric function and the plasmon dispersion of the Q2D EL. With this information, the self-energy, quasiparticle lifetime, mobility etc., can also be obtained; polarons in Q2D systems can be studied with the inclusion of electron-electron screening.

## **ACKNOWLEDGMENTS**

We gratefully acknowledge discussions with N. Günalp, A. Gökalp, and K. Leblebicioğlu.

# APPENDIX A: TOTAL SYSTEM ENERGY IN THE VARIATIONAL APPROACH

In this section, for completeness we include the expression for the *total* system energy of a heterojunction in Bastard's variational approach [17]. The ground-state expectation of the total system energy per electron is

$$\langle \tilde{E}_{TOT}(b) \rangle = \langle T(b) \rangle + \frac{1}{2} \langle U_{e-e}(b) \rangle + \langle U_A(b) \rangle + \langle U_{barrier}(b) \rangle, \quad (29)$$

where  $\langle T(b) \rangle$  is the kinetic energy term given by

$$\langle T(b) \rangle = -\frac{M^2 \kappa_b}{4 m_B^*} + \frac{N^2}{2 m_A^* b} (1 + bz_0 - b^2 z_0^2 / 2) \text{ Ry}, \quad (30)$$

$\langle U_{e-e}(b) \rangle$  is the average electron-electron interaction potential,

$$\begin{aligned} \langle U_{e-e}(b) \rangle = & \frac{8\pi}{\epsilon} N_{2D} \left[ \frac{N^4}{b^7} \left( \frac{33}{4} + \frac{25bz_0}{2} + \frac{17b^2z_0^2}{2} + 3b^3z_0^3 + \frac{b^4z_0^4}{2} \right) \right. \\ & \left. - \frac{N^2 M^2}{\kappa_b^2 b^3} (z_0^2 b^2 + 2bz_0 + 2) \right] \text{ Ry}, \end{aligned} \quad (31)$$

where  $\langle U_A(b) \rangle$  is the average electron-ionized acceptor interaction potential,

$$\langle U_A(b) \rangle = \frac{8\pi}{\epsilon} N_{depl} \left[ \frac{6N^2}{b^4} \left( 1 + \frac{2}{3}bz_0 + \frac{b^2z_0^2}{6} \right) - \frac{M^2}{\kappa_b^2} \right] \text{ Ry}, \quad (32)$$

where  $\langle U_{barrier}(b) \rangle$  is the average potential energy due to step-barrier,

$$\langle U_{barrier}(b) \rangle = \frac{U_{b,Ry} N^2 z_0^2}{\kappa_b} \text{ Ry}, \quad (33)$$

where  $\kappa_b = 2\sqrt{m_B^* U_{b,Ry}}$ . In above equations atomic units are used; all energies are in Rydbergs ( $1\text{Ry} = m_0 e^4 / 2\hbar^2$ ) and lengths in Bohr radius ( $a_B = \hbar^2 / m_0 e^2$ ). In the

*total* system energy, the electron-electron interaction is weighted by 1/2 to avoid double-counting. The variational parameter  $b$  is determined by minimizing  $\langle \tilde{E}_{TOT}(b) \rangle$  which is an easy task numerically as the cost function has a single minimum.

## APPENDIX B: EFFECTIVE 2D COULOMB INTERACTION

We first recall the electrostatic potential due to a point charge  $Q$ , at a distance  $d$  (along the  $z$ -axis) from the interface formed by two semi-infinite dielectric media with permittivities  $\epsilon_A$  and  $\epsilon_B$ . Solution of the Poisson's equation subject to continuity requirements at the interface,  $z = 0$  results in an electrostatic potential of the form [33],

$$\Phi(\vec{R}, z) = \begin{cases} \frac{1}{\epsilon_A} \left( \frac{Q}{\sqrt{R^2+(d-z)^2}} + \frac{\epsilon_A - \epsilon_B}{\epsilon_A + \epsilon_B} \frac{Q}{\sqrt{R^2+(d+z)^2}} \right), & z \geq 0 \\ \frac{2}{\epsilon_A + \epsilon_B} \frac{Q}{\sqrt{R^2+(d-z)^2}}, & z \leq 0 \end{cases}. \quad (34)$$

This result will now be used in constructing the effective 2D Coulomb interaction energy between two (charge) distributions  $n(\vec{R}, z)$  and  $n(\vec{R}', z')$

$$\begin{aligned} U^{Q2D}(\vec{R} - \vec{R}') = & \\ & \frac{e^2}{\epsilon_A} \left\{ \int_0^\infty dz \int_0^\infty dz' \left[ \frac{n(\vec{R}, z) n(\vec{R}', z')}{\sqrt{|\vec{R} - \vec{R}'|^2 + (z - z')^2}} + \frac{\epsilon_A - \epsilon_B}{\epsilon_A + \epsilon_B} \frac{n(\vec{R}, z) n(\vec{R}', z')}{\sqrt{|\vec{R} - \vec{R}'|^2 + (z + z')^2}} \right] \right\} \\ & + \frac{e^2}{\epsilon_B} \left\{ \int_{-\infty}^0 dz \int_{-\infty}^0 dz' \left[ \frac{n(\vec{R}, z) n(\vec{R}', z')}{\sqrt{|\vec{R} - \vec{R}'|^2 + (z - z')^2}} + \frac{\epsilon_B - \epsilon_A}{\epsilon_A + \epsilon_B} \frac{n(\vec{R}, z) n(\vec{R}', z')}{\sqrt{|\vec{R} - \vec{R}'|^2 + (z + z')^2}} \right] \right\} \\ & + \frac{2e^2}{\epsilon_A + \epsilon_B} \left\{ \int_0^\infty dz \int_{-\infty}^0 dz' \frac{n(\vec{R}, z) n(\vec{R}', z')}{\sqrt{|\vec{R} - \vec{R}'|^2 + (z - z')^2}} + \int_{-\infty}^0 dz \int_0^\infty dz' \frac{n(\vec{R}, z) n(\vec{R}', z')}{\sqrt{|\vec{R} - \vec{R}'|^2 + (z - z')^2}} \right\} \end{aligned} \quad (35)$$

The first two terms in Eq. (35) represent direct and image interaction of the charge distributions on the right side of the interface ( $z > 0$ ). Third and fourth terms represent the same interactions for  $z < 0$  region. The last two terms which are in fact equal,

represent the direct interaction between charge distributions on opposite sides of the interface.

The charged-particle distribution is  $n(\vec{R}, z) \equiv n(z) = |\varsigma_1(z)|^2$ , where  $\varsigma_1(z)$  is given in Eq. (2). The 2D Fourier transform of  $U^{Q2D}(\vec{R} - \vec{R}')$  is easily obtained using the result

$$\int d^2r \frac{e^{-i\vec{q}\cdot\vec{r}}}{\sqrt{r^2 + a^2}} = \frac{2\pi}{q} e^{-|a|q} \quad (36)$$

as

$$U^{Q2D}(q) = \frac{2\pi e^2}{q\epsilon_A} \left( I_1 + \frac{\epsilon_A - \epsilon_B}{\epsilon_A + \epsilon_B} I_2 \right) + \frac{2\pi e^2}{q\epsilon_B} \left( I_3 + \frac{\epsilon_B - \epsilon_A}{\epsilon_A + \epsilon_B} I_4 \right) + \frac{8\pi e^2}{q(\epsilon_A + \epsilon_B)} I_5, \quad (37)$$

with,

$$I_1 = \int_0^\infty dz \int_0^\infty dz' N^4 (z + z_0)^2 (z' + z_0)^2 e^{-bz} e^{-bz'} e^{-|z-z'|q}, \quad (38)$$

$$I_2 = \int_0^\infty dz \int_0^\infty dz' N^4 (z + z_0)^2 (z' + z_0)^2 e^{-bz} e^{-bz'} e^{-(z+z')q}, \quad (39)$$

$$I_3 = \int_{-\infty}^0 dz \int_{-\infty}^0 dz' M^4 e^{\kappa_b(z+z')} e^{-|z-z'|q} \quad (40)$$

$$I_4 = \int_{-\infty}^0 dz \int_{-\infty}^0 dz' M^4 e^{\kappa_b(z+z')} e^{(z+z')q} \quad (41)$$

$$I_5 = \int_0^\infty dz \int_{-\infty}^0 dz' M^2 N^2 e^{\kappa_b z'} (z + z_0)^2 e^{-bz} e^{-(z-z')q}. \quad (42)$$

These integrals are straightforward and the results are listed in Eqs. (7)-(11). The effective 2D interaction  $U^{Q2D}(\vec{R} - \vec{R}')$  must reduce to ideal 2D case as  $|\vec{R} - \vec{R}'| \rightarrow \infty$ .

$$\lim_{|\vec{R}-\vec{R}'|\rightarrow\infty} U^{Q2D}(\vec{R} - \vec{R}') = \frac{e^2}{\epsilon_A |\vec{R} - \vec{R}'|} \left( 1 + \frac{\epsilon_A - \epsilon_B}{\epsilon_A + \epsilon_B} \right) \left[ \int_0^\infty dz n(z) \right]^2 + \frac{e^2}{\epsilon_B |\vec{R} - \vec{R}'|} \left( 1 + \frac{\epsilon_B - \epsilon_A}{\epsilon_A + \epsilon_B} \right) \left[ \int_{-\infty}^0 dz n(z) \right]^2 + \frac{4e^2}{(\epsilon_A + \epsilon_B) |\vec{R} - \vec{R}'|} \int_0^\infty dz n(z) \int_{-\infty}^0 dz' n(z'). \quad (43)$$

Using  $\int_0^\infty n(z) dz = 1 - \int_{-\infty}^0 n(z') dz'$  in Eq. (43) leads to the desired result,

$$\lim_{|\vec{R}-\vec{R}'|\rightarrow\infty} U^{Q2D}(\vec{R}-\vec{R}') = \frac{e^2}{|\vec{R}-\vec{R}'|} \frac{2}{\epsilon_A + \epsilon_B}. \quad (44)$$

As a consequence the Fourier transform gives

$$\lim_{q\rightarrow 0} U^{Q2D}(q) = \frac{2\pi e^2}{q\bar{\epsilon}}, \quad (45)$$

so that  $\lim_{q\rightarrow 0} F(q) = 1$  as can be observed in Fig. 1. This also indicates that all of the interactions are properly accounted in Eq. (37).

## References

- [1] K. S. Singwi and M. P. Tosi, in *Solid State Physics*, edited by F. Seitz, H. Ehrenreich, and D. Turnbull (Academic, New York, 1981), Vol. 36, p. 177.
- [2] H. M. Van Horn, Phys. Rev. **157**, 342 (1967); E. E. Salpeter and H. M. Van Horn, Astrophys. J. **155**, 183 (1969); E. Schatzman, in *Strongly Coupled Plasmas*, edited by G. Kalman (Plenum, New York, 1978), p. 407; E. Schatzman, J. Phys. (Paris) Suppl. **41**, C2 (1980).
- [3] T. Ando, A. B. Fowler, and F. Stern, Rev. Mod. Phys. **54**, 437 (1982).
- [4] For reviews, see, S. Hiyamizu, Semicond. Semimet. **30**, 53 (1990); H. Morkoç, *The Technology and Physics of Molecular Beam Epitaxy* (Plenum, New York, 1985), p. 185.

- [5] See, for instance, M. S. Dresselhaus and G. Dresselhaus, *Adv. Phys.* **30**, 139 (1981); H. M. Miesenböck and M. P. Tosi, *Z. Phys. B* **78**, 255 (1990).
- [6] For a collection of papers see, M. Stone (editor) *Quantum Hall Effect* (World Scientific, Singapore, 1992); also see, T. Chakraborty and P. Pietiläinen, in *The Fractional Quantum Hall Effect*, Springer Series in Solid-state Sciences Vol. 85 (Springer-Verlag, Berlin, 1988).
- [7] F. Stern, *Phys. Rev. Lett.* **18**, 546 (1967).
- [8] M. Jonson, *J. Phys. C* **9**, 3055 (1976).
- [9] K. S. Singwi, M. P. Tosi, R. H. Land, and A. Sjölander, *Phys. Rev.* **176**, 589 (1968).
- [10] B. Tanatar, and D. M. Ceperley, *Phys. Rev.* **B39**, 5005 (1989).
- [11] C. Bulutay and M. Tomak, *Phys. Rev.* **B53**, 7317 (1996).
- [12] G. Mahan, *Many-Particle Physics*, 2nd ed. (Plenum, New York, 1990).
- [13] See, for instance, L. Hedin and B. I. Lundqvist, *J. Phys. C* **4**, 2064 (1971); R. M. Dreizler and E. K. U. Gross, *Density Functional Theory* (Springer-Verlag, Heidelberg, 1990), p. 149.
- [14] S. Das Sarma, *Phys. Rev.* **B27**, 2590 (1983).
- [15] S. Das Sarma and B. A. Mason, *Phys. Rev.* **B31**, 5536 (1985).

- [16] W. Xiaoguang, F. M. Peeters, and J. T. Devreese, Phys. Stat. Sol. (b)**133**, 229 (1986).
- [17] G. Bastard, *Wave Mechanics Applied to Semiconductor Heterostructures* (Les Editions de Physique, Cedex, 1988), p. 155; G. Bastard, Surf. Sci.**142**, 284 (1984); M. Ayman Magdy, R. A. Al-Khader, and M. Tomak, Nuovo Cimento D**17**, 357 (1995) and references therein.
- [18] F. J. Fernández-Velicia, F. García-Moliner, and V. R. Velasco, Phys. Rev. B**53**, 2034 (1996).
- [19] A. Gold and L. Calmels, Phys. Rev. B**48**, 11622 (1993).
- [20] See, for e.g., N. Iwamoto, Phys. Rev. B**43**, 2174 (1991).
- [21] G. Barton, *Elements of Green's Functions and Propagation: potentials, diffusion and waves* (Clarendon, New York, 1989).
- [22] J. S. Thakur and K. N. Pathak, J. Phys. C: Solid State Phys.**16**, 6551 (1983).
- [23] D. Olego, A. Pinczuk, A. C. Gossard, and W. Wiegmann, Phys. Rev. B**26**, 7867 (1982).
- [24] A. Isihara, Solid State Phys. **42**, 271 (1989).
- [25] F. Stern and S. Das Sarma, Phys. Rev. B**30**, 840 (1984).

- [26] M. O. Watanabe, J. Yoshida, M. Mashita, T. Nakanisi, and A. Hojo, *J. Appl. Phys.* **57**, 5340 (1985); T. W. Hickmott, P. M. Solomon, R. Fischer, and H. Morkoç, *J. Appl. Phys.* **57**, 2844 (1985); D. Arnold, A. Kettensen, T. Henderson, J. Klem, and H. Morkoç, *J. Appl. Phys.* **57**, 2880 (1985).
- [27] J. P. Eisenstein, L. N. Pfeiffer, and K. W. West, *Phys. Rev. B* **50**, 1760 (1994).
- [28] D. Heitmann, *Phys. Scripta* **T25**, 294 (1989) and references therein.
- [29] J. J. Baumberg, and D. A. Williams, *Phys. Rev. B* **53**, R16140 (1996).
- [30] D. Pines, *Elementary Excitations in Solids* (Benjamin, New York, 1963).
- [31] G. D. Mahan, *Phys. Scripta* **32**, 423 (1985).
- [32] S. Moroni, D. M. Ceperley, and G. Senatore, *Phys. Rev. Lett.* **69**, 1837 (1992).
- [33] J. D. Jackson, *Classical Electrodynamics* (Wiley, New York, 1975), p. 147.

## List of Tables

1. Fitting parameters  $A$ ,  $B$ ,  $C$ , and  $D$  used in Eqs. (22) and (24) as a function of  $r_s$  for the characterization of the Q2D EL in a GaAs/AlGaAs heterostructure. The ionized acceptor density is  $N_{depl} = 0.46 \times 10^{11} \text{ cm}^{-2}$ . See Sec. IV for the other parameters used for GaAs/AlGaAs system.
2. The constants used in Eqs. (25)-(28) for different ionized acceptor densities,  $N_{depl}$ . The parameters characterizing the heterostructure are chosen suitable to the GaAs/AlGaAs system (see Sec. IV).

## List of Figures

1. The Coulomb form factor  $F$  and the effect of the image terms as a function of wave number  $q$  (in units of  $k_F$ ) for the electronic densities  $r_s=0.8$  and 20. The full lines apply to GaAs/AlGaAs heterostructure having  $\epsilon_A=13$  and  $\epsilon_B=12.1$ . The dashed lines refer to the same system but with  $\epsilon_A = \epsilon_B=12.55$  so that no image term appears. See Sec. IV for the definition of  $r_s$  and other parameters used for the system.
2. The local-field correction,  $G^{Q2D}(q)$  of Q2D EL versus wave number  $q$  (in units of  $k_F$ ) for  $r_s$  values 0.8, 1, 2, 3, 4, 5, 10, 15, and 20. Solid lines: STLS and dashed lines: calculation using the fitted form for  $G^{Q2D}(q)$ ; see Eq. (22) with the values from Table I.
3. The comparison of the full STLS Q2D local-field correction (solid lines) with that of Gold and Calmels' (dashed lines) given by Eq. (15) as a function of wave number  $q$  (in units of  $k_F$ ) for  $r_s=1$  and 10.
4. Comparison of ideal 2D and Q2D inverse static dielectric function,  $1/\epsilon(q, 0)$  as a function of wave number  $q$  (in units of  $k_F$ ) for  $r_s=3$ . Solid lines: STLS, dashed lines: RPA. For Q2D EL, GaAs/AlGaAs heterostructure is used with  $N_{depl} = 0.46 \times 10^{11} \text{ cm}^{-2}$ .
5. The effect of the barrier height,  $U_b$  on the inverse static dielectric function,  $1/\epsilon(q, 0)$  as a function of wave number  $q$  (in units of  $k_F$ ) for  $r_s=0.8$ . Solid line:  $U_b = 0.1 \text{ eV}$ ,

dashed line:  $U_b \rightarrow \infty$ . Other parameters for the heterostructure are given in Sec. IV.

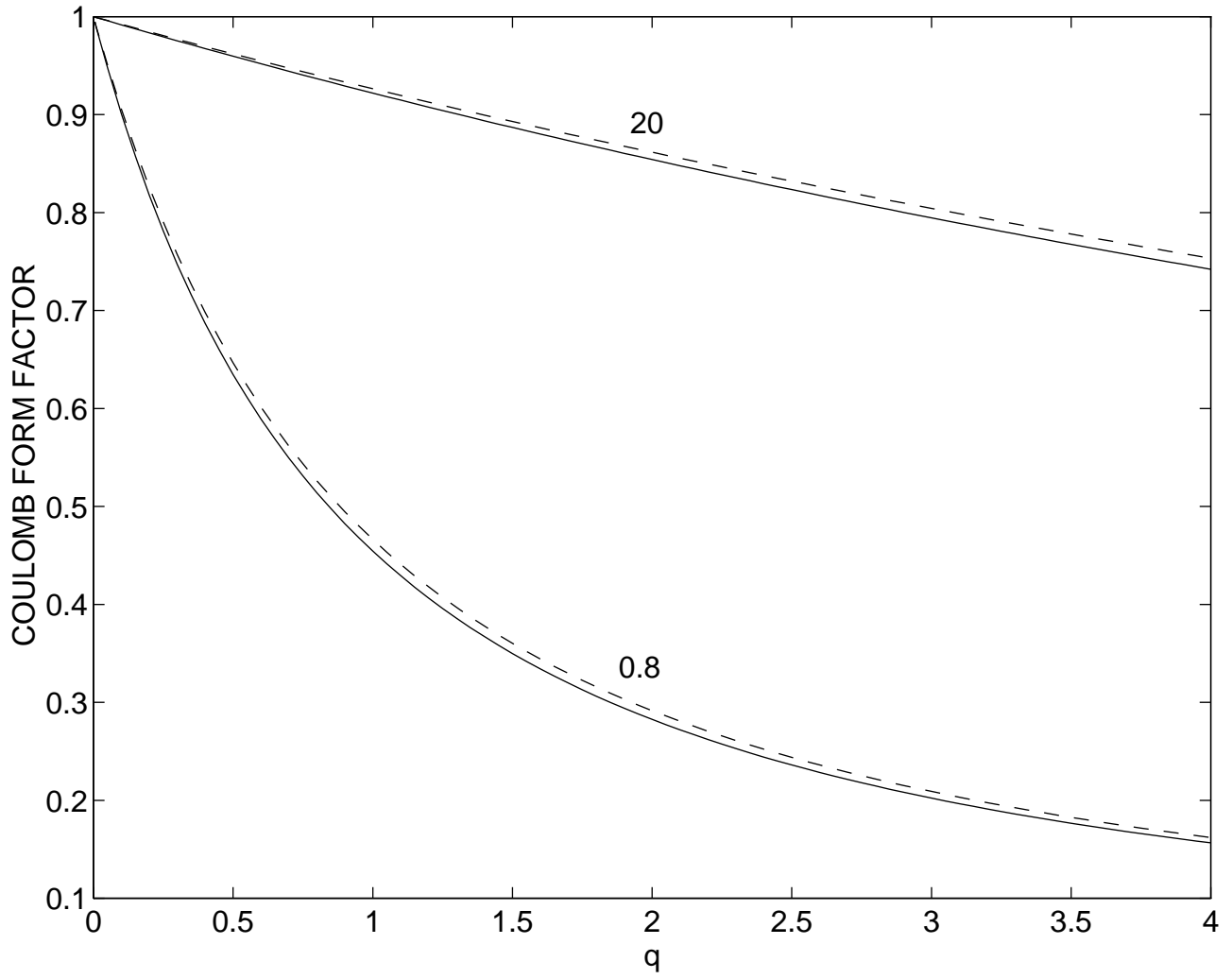
6. The inverse static dielectric function of Q2D EL,  $1/\epsilon(q, 0)$  as a function of wave number  $q$  (in units of  $k_F$ ) for  $r_s$  values 0.8, 1, 2, 3, 4, 5, 10, 15, and 20. Solid lines: STLS and dashed lines: calculation using the fitted forms for  $G^{Q2D}(q)$  given by Eq. (22) and  $F(q)$  given by Eq. (24) with the values in Table I.
  
7. The electron distribution along the confinement direction in arbitrary units. The total electron density is  $1 \times 10^{12} \text{ cm}^{-2}$ . Other parameters are given in Sec. IV. Solid line refers to the two subband populated calculation and the dashed line is based on the electrical quantum limit.
  
8. The normalized plasmon energy ( $E_p/E_F \equiv 2\nu_p$ ) as a function of wave number  $q$  (in units of  $k_F$ ) for  $r_s$  values 1, 5, 10, and 20. Solid lines: STLS and dashed lines: calculation using the fitted forms for  $G^{Q2D}(q)$  given by Eq. (22) and  $F(q)$  given by Eq. (24) with the values in Table I. The dotted line marks the onset of the electron-hole continuum.

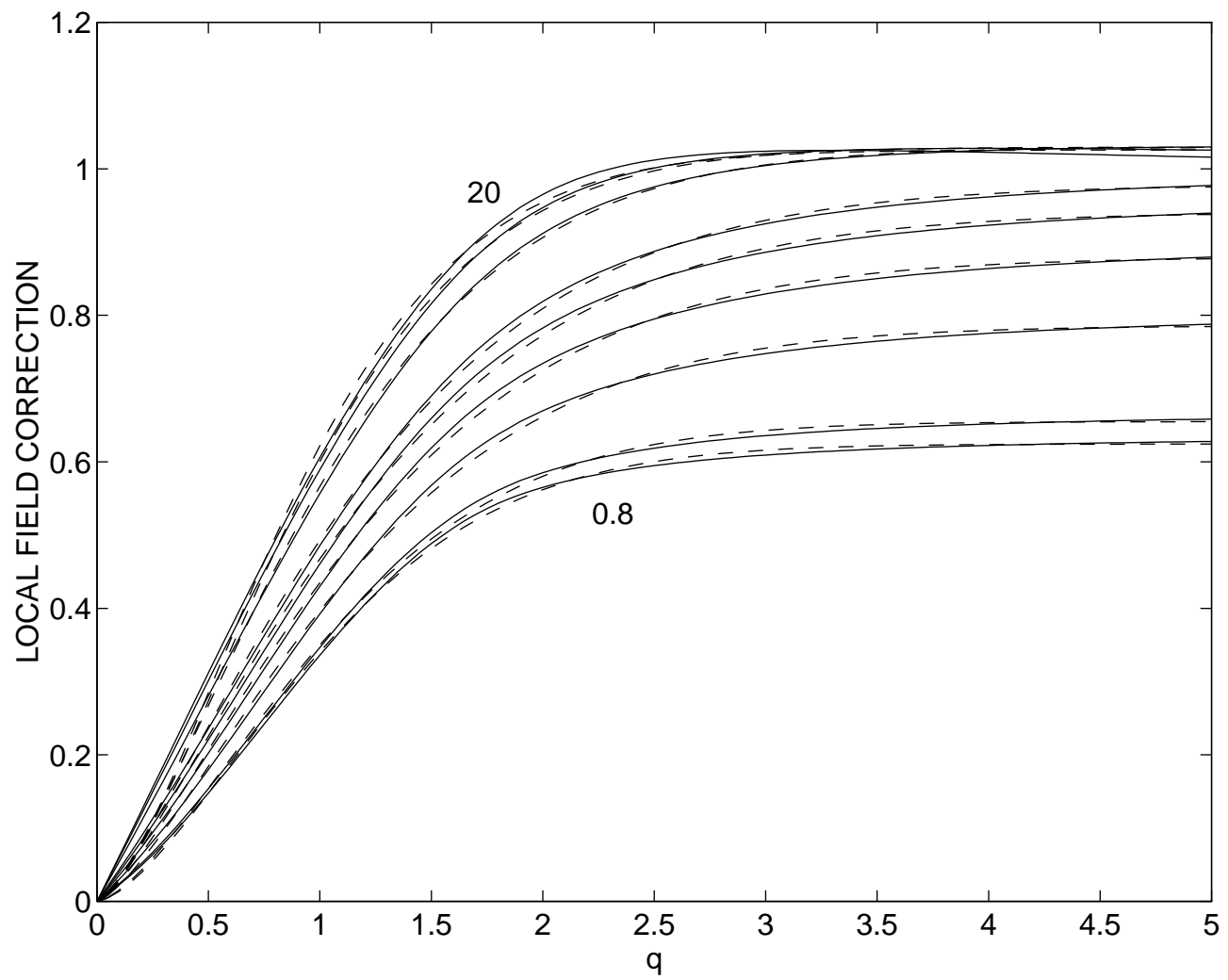
$r_s$	$A$	$B$	$C$	$D$
0.8	0.6243	0.4923	1.5462	1.2750
1.0	0.6549	0.5005	1.5079	1.1542
1.5	0.7250	0.5274	1.4342	0.9285
2.0	0.7857	0.5519	1.3950	0.7690
2.5	0.8380	0.5763	1.3644	0.6497
3.0	0.8794	0.5999	1.3512	0.5571
4.0	0.9405	0.6461	1.3274	0.4321
5.0	0.9779	0.6855	1.3264	0.3494
6.0	1.0012	0.7209	1.3356	0.2922
8.0	1.0225	0.7792	1.3683	0.2197
10	1.0294	0.8223	1.4097	0.1752
12	1.0305	0.8597	1.4545	0.1454
15	1.0295	0.9007	1.5014	0.1158
20	1.0257	0.9555	1.5185	0.0863

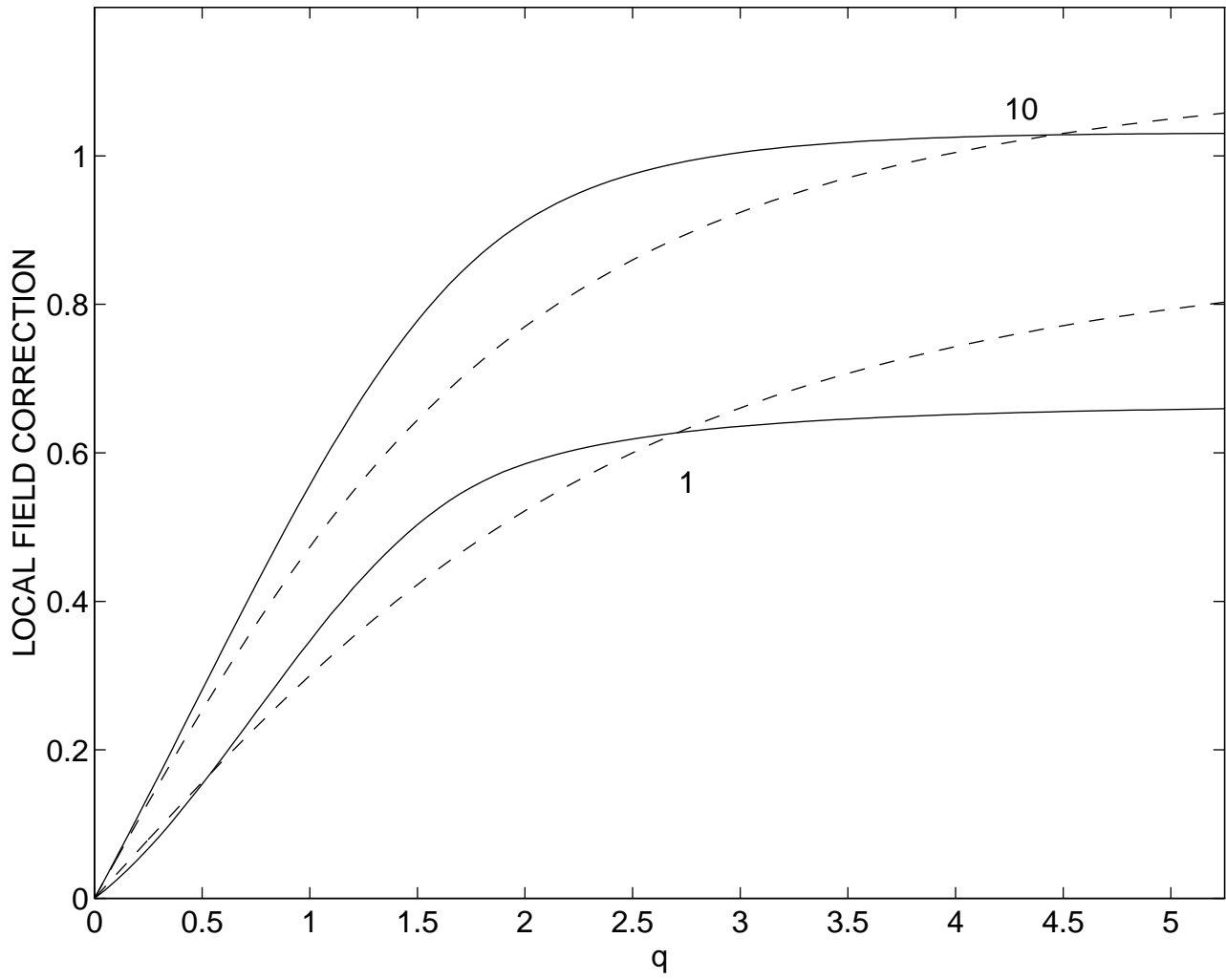
Table 1:

$N_{depl} (\text{cm}^{-2})$	$a_1$	$a_2$	$a_3$	$b_1$	$b_2$	$b_3$	$c_1$	$d_1$	$d_2$
$0.146 \times 10^{11}$	0.6384	0.2213	0.5555	0.3023	4.9907	-0.0435	0.6891	4.3194	2.4659
$0.46 \times 10^{11}$	0.6770	0.2794	0.6372	0.2575	2.6283	0.1623	0.7914	2.7325	1.3674
$1.47 \times 10^{11}$	0.6953	0.2302	0.6888	0.2253	1.4913	0.3043	1.1675	1.6566	0.6898
$4.69 \times 10^{11}$	0.6887	0.1802	0.7418	0.1978	0.6977	0.4195	1.5437	1.0004	0.3518

Table 2:







# INVERSE STATIC DIELECTRIC FUNCTION

